PROCEEDINGS OF THE ROYAL SOCIETY A

Proc. R. Soc. A (2012) **468**, 1496–1520
doi:10.1098/rspa.2011.0731
Published online 1 February 2012

Double twinning mechanisms in magnesium alloys via dissociation of lattice dislocations

By I. J. Beyerlein[1,*], J. Wang[2], M. R. Barnett[3] and C. N. Tomé[2]

[1] *Theoretical Division, and* [2] *Materials Science and Technology Division, Los Alamos National Laboratory, Los Alamos, NM 87545, USA*
[3] *Centre for Material and Fibre Innovation, ITRI, Deakin University, Geelong, Victoria 3217, Australia*

In this work, we propose dislocation mechanisms for the formation of $\{10\bar{1}1\}-\{10\bar{1}2\}$ double twin structures in hexagonal close packed (HCP) crystals through the nucleation of secondary twins within primary twin domains. The model considers that secondary twins associated with the most commonly observed double twin variants (i.e. type 1 and type 2) nucleate and thicken by a sequence of three distinct dissociation reactions of mixed basal dislocations. Provided that the less frequently observed double twin variants (i.e. type 3 and type 4) also form by a dislocation-based mechanism, we show that their development must proceed by a separate set of dissociation reactions involving pyramidal $\langle c + a \rangle$ slip dislocations. Mechanistic, crystallographic and energetic considerations indicate that the type 1 variant should be the most prevalent. The mechanisms proposed here would also apply to the analysis of $\{10\bar{1}3\}-\{10\bar{1}2\}$ compound twins and HCP metals other than Mg that exhibit double twinning, such as titanium.

Keywords: twinning; magnesium; hexagonal close packed

1. Introduction

A phenomenon particularly influential in the deformation, fatigue and fracture of magnesium (Mg) alloys at room temperature and above is double twinning (Reed-Hill & Robertson 1957*a*,*b*; Crocker 1962; Wonsiewicz & Backofen 1967; Yoshinaga *et al.* 1973; Ando *et al.* 2010; Koike *et al.* 2010). In the case of Mg, the most frequently observed double twin compositions are secondary $\{10\bar{1}2\}$ twins within primary $\{10\bar{1}1\}$ twins or $\{10\bar{1}3\}$ twins (Couling *et al.* 1959; Reed-Hill 1960; Yoshinaga *et al.* 1973). The formation of double twins has been correlated with the onset of localization and fracture (Couling & Roberts 1956; Hauser *et al.* 1956; Reed-Hill & Robertson 1957*b*; Yoshinaga *et al.* 1973; Ando *et al.* 2010). This correlation probably arises because the double-twinned region is much more favourably oriented for easy basal slip than the original parent crystal (Barnett *et al.* 2008). The intense basal slip activity that results within the thin plate-like region of the double twin produces a localized shear that cannot be accommodated across the primary twin interface and leads to cracking (Reed-Hill & Robertson 1957*b*; Hartt & Reed-Hill 1968; Cizek & Barnett 2008).

*Author for correspondence (irene@lanl.gov).

Received 15 December 2011
Accepted 4 January 2012

$\{10\bar{1}1\}-\{10\bar{1}2\}$ (or $\{10\bar{1}3\}-\{10\bar{1}2\}$) double twins initiate under stress states that favour the formation of $\{10\bar{1}1\}$ or $\{10\bar{1}3\}$ twins, which are contraction twins, activated when the hexagonal close packed (HCP) crystal experiences compressive stress along its *c*-axis (Couling & Roberts 1956; Reed-Hill & Robertson 1957*a*,*b*; Reed-Hill 1960; Partridge 1967; Akhtar 1973; Wang *et al.* 2011*a*). The secondary twin $\{10\bar{1}2\}$ is an extension twin, activated in *c*-axis tension (Partridge 1967; Akhtar & Teghtsoonian 1971; Wang *et al.* 2009*a*,*b*, 2010). A stress state that favours the nucleation of primary contraction twinning will also support secondary extension twinning within the primary twin domain.

Currently, we are faced with the problem of understanding and predicting which variant of double twin forms. Each HCP twin family contains six crystallographically equivalent twin variants. This means that for each primary contraction twin, there are six possible secondary extension twin variants that can form a double twin, of which four are crystallographically distinct. Experimental observations show that one double twin type is clearly more detrimental to ductility than the other three.

The usual approach for explaining variant selection has been to compare resolved shear stresses (or Schmid factors) on all possible secondary twin variants as a result of the applied stress state. Such an approach, however, does not take into account the complexity of the local stress state inside or in the vicinity of the primary twin (Aydiner *et al.* 2009) or the mechanisms required for nucleating the secondary twin. As a consequence, the results have proved inconsistent with experimental observations. Recent studies have found that one double twin type occurs most frequently (Barnett *et al.* 2008; Martin *et al.* 2010) and its prevalence is not driven entirely by the macroscopic applied stress (i.e. Schmid factors). The peculiar variant selection has since been rationalized based on accommodation mechanisms that apply well after the twin has nucleated. While seeking to explain how a secondary twin grows is important, it is also necessary, as a complement, to understand how it nucleates in the first place.

In a previous work, we also found that Schmid factor analyses did not explain variant selection observed for primary $\{10\bar{1}2\}$ twins in Mg and zirconium (Zr) (Capolungo *et al.* 2009*a*,*b*; Beyerlein *et al.* 2010). In this case, successfully predicting variant selection was possible only by modelling the mechanisms responsible for twin nucleation (Beyerlein & Tomé 2010; Beyerlein *et al.* 2011). In the same way, unravelling the mechanisms for secondary twin nucleation in double twinning should help explain double twin variant selection. Naturally, a particular twin variant will grow only if its twin embryo can form, and if the local stresses support its initial expansion. To our knowledge, the only existing nucleation theory for double twinning is the one proposed by Mendelson (1970), which, as we will discuss shortly, has its limitations.

Fundamental to understanding twin nucleation and growth is knowledge of the elementary defect responsible for twinning—the twinning dislocation (Hirth & Lothe 1982; Christian & Mahajan 1995). A twinning dislocation was first graphically conceptualized by Thompson & Millard (1952), which was then followed by analytical studies by Kronberg (1961) and Westlake (1966). Its structure, nucleation and motion were later numerically examined using molecular statics, molecular dynamics (MD) and *ab initio* simulation models (Serra *et al.* 1988, 1991; Wang *et al.* 2009*a*,*b*, 2011*a*). A formal topological theory of twinning dislocations was developed by Pond & Hirth (1994), where a twinning dislocation

was classified as a disconnection characterized by a dislocation Burgers vector **b** and step height h (encompassing n atomic layers). The values for **b** and h differ between the distinct types of HCP twins. These and other basic characteristics of twinning dislocations for the HCP twin types considered in this work (e.g. $\{10\bar{1}1\}$, $\{10\bar{1}2\}$ and $\{10\bar{1}3\}$) have been determined experimentally (Reed-Hill & Robertson 1957*a*; Reed-Hill 1960; Serra *et al.* 1991; Christian & Mahajan 1995; Pond *et al.* 1995; Li *et al.* 2010). Particularly in geometrically complex structures such as HCP lattices, the motion of twinning dislocations involves shear along with some small corrective shuffling (Serra *et al.* 1988, 1991; Wang *et al.* 2009*a*,*b*, 2011*a*). It should be mentioned that a shuffle-dominated twinning mechanism has been recently proposed as having disproved the concept of a twinning dislocation (Li & Ma 2009). However, the problems with this claim were later discussed by Serra *et al.* (2010). For this work, it suffices to point out that the well-supported and widely accepted classical twinning dislocation model has enabled explanations of twin nucleation from grain boundaries (Wang *et al.* 2010) or at the head of pile ups (Mendelson 1969, 1970; Capolungo & Beyerlein 2008), twin transmission across interfaces (Wang *et al.* 2011*b*), twin boundary migration (Serra & Bacon 1996; Wang *et al.* in press), and the apparent non-Schmid effects on variant selection (Beyerlein & Tomé 2010; Beyerlein *et al.* 2011).

Using dislocation theory and considering HCP crystallography, we propose in the present work a set of nucleation mechanisms for all possible secondary twin variants. This study seeks to explain the nucleation of the secondary twin at the primary twin interface and its early stages of growth into the primary twin domain. Consistent with previous experimental observations, our approach reveals that the nucleation of one variant is undoubtedly more energetically favourable than the rest.

(*a*) *Classification of double twin variants: types 1–4*

The six possible secondary twin variants create four crystallographically distinct double twin variants, conventionally referred to as type 1–4 (Yoshinaga *et al.* 1973; Barnett *et al.* 2008). Figure 1 shows the geometrical relationship between a primary twin boundary and the six secondary twin planes corresponding to (i) types 1 and 2, (ii–iii) type 3 and (iv–v) type 4 within an HCP unit cell.

Types 1 and 2 double twins share the same zone axis with the primary twin, which lies along AB in figure 1, and account for secondary twinning by two of the six possible $\{10\bar{1}2\}$ twin variants (figure 1*a*). The secondary twin plane ABde corresponds to type 1 and plane ABd′e′ to type 2.

Figure 2 shows the crystallographic relationship between the type 1 and 2 double twin systems and the primary twin. Figure 2*a* delineates the crystallographic relationship of the type 1 and 2 secondary twin planes with respect to each other on the same side of a primary $(\bar{1}011)$ twin boundary plane, and figure 2*b* shows type 1 and type 2 double twins with some finite thickness, with its reoriented basal planes marked. The misorientation angle about the common zone axis between the basal planes of the parent and type 1 or type 2 structure is 37.5° or 30.1°, respectively, for Mg (Crocker 1962; Barnett *et al.* 2008).

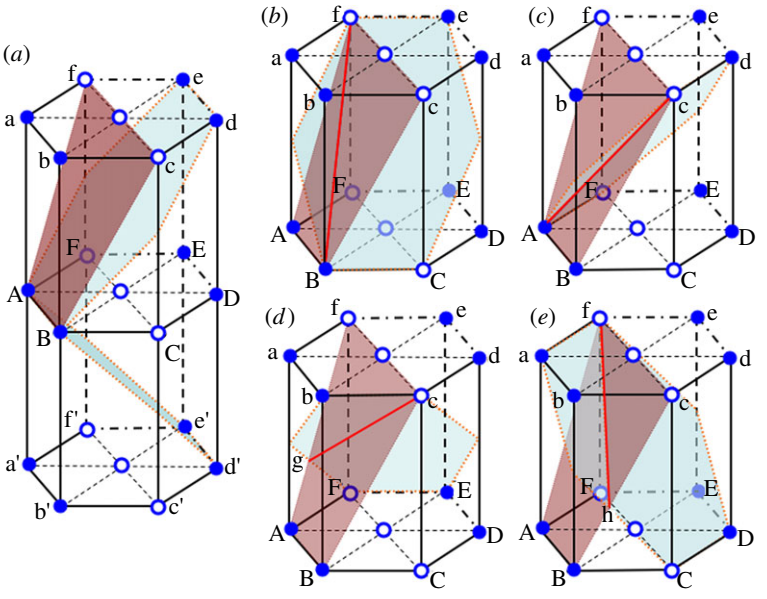

Figure 1. The geometrical relationship between each of the six secondary $\{10\bar{1}2\}$ twin planes (light blue) and a given primary $\{10\bar{1}1\}$ twin boundary (dark red). (*a*) Twin plane ABde corresponds to type 1 and ABd′e′ to type 2. Both share the same zonal axis along AB with the primary twin. (*b*,*c*) Two variants of type 3. The intersection lines in red of the primary and secondary twin planes lie along (*b*) Bf or (c) Ac. (*d*,*e*) Two variants of type 4. The red intersection lines of the primary and secondary twin planes lie along (*d*) cg or (*e*) fh.

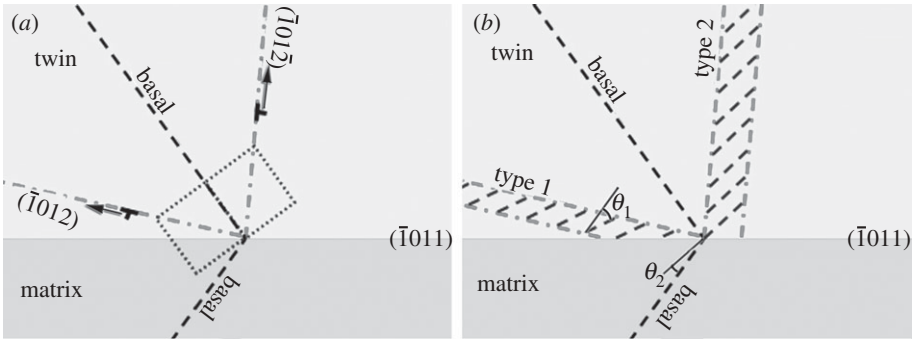

Figure 2. (*a*) Schematic of the crystallographic relationship of the type 1 and 2 secondary twin variants with respect to a primary $(\bar{1}011)$ twin boundary. (*b*) Type 1 and 2 twins with the basal planes delineated show that the misorientation angle between the basal planes of the parent and the type 1 or type 2 twin about the zone axis is $\theta_1 = 37.5°$ or $\theta_2 = 30.1°$, respectively (Barnett *et al.* 2008).

In contrast, secondary twin variants associated with types 3 and 4 have a zone axis non-parallel to that of the primary twin. The two twin planes (BCef and AcdF) in figure 1*b*,*c* produce a type 3 double twin structure. The primary

and secondary twin planes intersect along Bf in figure 1*b* and Ac in figure 1*c*. Both variants of type 3 create a 66.5° misorientation angle (for Mg) between the basal planes of the parent matrix- and doubly twinned lattice. Double twin configurations involving secondary twinning on the remaining two planes—EFbc and CDfa in figure 1*d*,*e*—create a type 4 double twin structure. The intersection lines of the primary and secondary twin planes lie along cg in figure 1*d* and fh in figure 1*e*. The misorientation angle for these two variants of type 4 is 69.9° for Mg.

All double twin types have been identified in deformed Mg alloys via electron backscattering diffraction (EBSD) or transmission electron microscopy analyses (Barnett *et al.* 2008; Cizek & Barnett 2008; Ando *et al.* 2010; Martin *et al.* 2010). Type 1 is the most frequently observed, even in situations in which the type 1 secondary twin variant is unfavourably oriented with respect to the applied loading (Yoshinaga *et al.* 1973; Barnett *et al.* 2008; Martin *et al.* 2010). Significantly, it is also the most favourable for localization of basal slip, leading to potential failure (Barnett *et al.* 2008; Ando *et al.* 2010). The other types of double twinning systems have been observed experimentally via EBSD, albeit in smaller portions than type 1 (Barnett *et al.* 2008; Martin *et al.* 2010).

Understanding what governs selection of the secondary twin variant requires knowing the mechanisms behind double twinning. Double twinning was first studied crystallographically by Crocker (1962) who presented a theory to predict the habit plane of various compositions of double twins. His treatment is two-dimensional and applies to types 1 and 2, in which the two component twins share the same zone axis (or twin plane of shear). Favourable comparisons with measurement confirmed the theory's assumption that the distortions accompanying double twinning can be described by an invariant plane strain, where the interface between the doubly twinned structure and the parent remains unstrained and plane. Thus, physically, the nucleation and growth processes involved in re-twinning the primary twin do not require additional accommodation via deformation of the surrounding crystal or the double-twinned region or both. Yoshinaga *et al.* (1973) proposed another mechanism for the development of the double twin boundary plane based on basal dislocation emission from the twin boundary. To date, only Mendelson (1970) has put forth a nucleation theory for double twinning. He proposed that $\langle c \rangle$ and $\langle c + a \rangle$ slip dislocations interact with and dissociate at the primary twin boundary, providing multiple $\{10\bar{1}2\}$ twinning dislocations inside the primary twin domain. Although a possible mechanism, it assumes operation of a hard $\langle c + a \rangle$ slip system or chance encounters with sessile $\langle c \rangle$ dislocations. The analysis was also confined to the case in which the primary and secondary twin shared the same zone axis (i.e. type 1 and type 2). Explanations for type 1 dominance must be based on an analysis of all four types, which was performed by Barnett *et al.* (2008) and Martin *et al.* (2010). There, reasons were offered based on the amount of strain required to accommodate a double twin that has already grown to micron thicknesses with the conclusion that type 1 requires the least. This arguably addresses growth but not nucleation and both aspects should be considered. To date, questions remain regarding what triggers secondary twinning and how the nucleation process may differ among types 1–4. It is the goal of the present work to study the nucleation aspect to help shed light on why type 1 is favoured over the others and why double twinning occurs in the first place.

(*b*) *Heterogeneous nucleation of secondary twins by dissociation of dislocations at the primary twin boundary*

In this work, we propose mechanisms for the formation of all four double twin types, an undertaking which has not been attempted previously. For all twin types, secondary twin nucleus formation and initial expansion within the primary twin domain involve a sequence of reactions that initiate when slip dislocations intersect a twin boundary and dissociate into twinning dislocations. However, for reasons that will be given shortly, separate mechanisms are presented for type 1/type 2 and type 3/type 4 $\{10\bar{1}2\}$ secondary twinning within a primary twin, both based on dislocation theory. The remainder of the work is structured as follows. After a brief background on dissociation reactions in §2, we describe in §3 the proposed mechanism and corresponding dissociation reactions for types 1 and 2 in detail, because they are the more frequently observed double twin variants. Section 4 follows with the associated energetics. We then present in §5 the mechanism for type 3 and 4 double twins. We end with a discussion on double twin variant selection in §6.

Throughout this paper, we will focus on the $\{10\bar{1}1\}$–$\{10\bar{1}2\}$ double twin composition, although the concepts can be easily translated to the $\{10\bar{1}3\}$–$\{10\bar{1}2\}$ composition. The reason is that the $\{10\bar{1}3\}$ twinning dislocation is fundamentally similar in character, topology and atomic displacements to the $\{10\bar{1}1\}$ twinning dislocation (Wang *et al.* 2011*a*). In the following, we use Mg as a technically relevant example, although the mechanisms apply generally to double twinning in any HCP solid, such as Ti (Bozzolo *et al.* 2010).

2. Basic characteristics of the dissociations and twinning partials involved

It is important that we first provide some background on the dissociation reactions that convert lattice dislocations to twinning dislocations and the particular defects involved in the mechanisms proposed here.

Certain geometrical and energetic constraints define the set of possible dissociation reactions that can produce twinning dislocations (Mendelson 1969, 1970). (i) All dislocations must share the same zone axis. (ii) In any dissociation, the Burgers vector must be conserved. (iii) The Burgers vector and twin plane must correspond to a glissile twinning dislocation. (iv) The total resolved shear stress acting on the twinning dislocations repels it away from the reaction site. It will be demonstrated that all reactions proposed in this work satisfy these constraints.

The interaction force between the dislocations produced from the dissociations is proportional to the dot product of their Burgers vectors (Hirth & Lothe 1982). A positive dot product indicates a repulsive interaction, which will favour the dissociation reaction. However, to determine if the dissociation is energetically favourable, the imposed stress field and twin boundary energy should also be taken into account. To this end, the energy changes before and after each reaction will be discussed later in §4.

Constraint (i) and geometrical differences among the different double twin types dictate that the slip dislocations that dissociate are not the same for types 1–2 and types 3–4. As shown in figure 1*a*, the common zone axis of the type

1 and 2 secondary twin planes and the primary twin boundary plane lie in the basal plane. This geometrical coincidence is important because it implies that these secondary twin variants could nucleate from a reaction of basal dislocations that glide into the primary twin boundary. The twins involved in type 3 and 4 doubly twinned structures do not share the same plane of shear and, hence the corresponding secondary twins must be created by a different set of dissociations reactions than those for types 1 and 2. Unlike types 1 and 2, the intersection lines between the primary and secondary twin planes for both types 3 and 4 do not lie in the basal plane (figure 1*b–e*). Thus, secondary twinning dislocations cannot be produced from the dissociation of basal dislocations interacting with the primary twin boundary. Their creation must entail dislocations belonging to the less favourable $\langle c+a\rangle$ slip modes, which for Mg are all harder to activate than basal slip. This structural difference provides some preliminary explanation regarding why types 3 and 4 double twin variants appear infrequently compared to type 1. It also suggests that these uncommon variants may become possible when basal slip within the primary twin is not favourable or the resolved shear stresses on the secondary $\{10\bar{1}2\}$ twin systems associated with types 1 and 2 are comparatively low.

Dissociation reactions will be written symbolically, using boldface symbols, in terms of the Burgers vectors involved. The Burgers vector of the three possible *mixed* basal dislocations will be denoted as $\mathbf{B}$. For each primary twin variant, only two out of three basal dislocations share the same zone axis as the primary twin. These two basal dislocations have the same edge component, whose Burgers vector is denoted by $\mathbf{B_e}$, but opposing screw components $\mathbf{B_s}$. Only $\mathbf{B_e}$ affects the character of the product twinning dislocations, and thus the twinning partial(s) are the same for the two mixed dislocations associated with the zone axis.[1] Table 1 lists the specific dislocations associated with each zone axis. The Burgers vectors of $\langle c+a\rangle$ pyramidal slip dislocations b_{py} are given by $[\mathbf{B}\pm\mathbf{C}]$, where $\mathbf{C}=c[0001]$. The Burgers vector of the twinning dislocations can be expressed as a fraction s of the twinning direction $\boldsymbol{\eta}_1$, which in turn, can be written in terms of $\mathbf{B_e}$ and $\mathbf{C}$ (Mendelson 1970). The edge components of the Burgers vectors of $\{10\bar{1}1\}$ and $\{10\bar{1}2\}$ twinning partials are $s_1[3\mathbf{B_e}\pm 2\mathbf{C}]$ and $s_2[3\mathbf{B_e}\pm\mathbf{C}]$, respectively. The values of s_1 and s_2 depend on the number n of crystallographic planes affected by each partial. For an elementary $\{10\bar{1}2\}$ twinning dislocation, $n=2$ (Serra *et al.* 1988, 1991; Wang *et al.* 2009*a*). For an elementary $\{10\bar{1}1\}$ twinning dislocation, it is commonly assumed in analytical modelling that $n=4$ (Rosenbaum 1964; Mendelson 1969, 1970; Yoo 1969); however, the issue on whether $n=2$ or $n=4$ has historically encountered some controversy (Westlake 1961, 1966; Thornton 1965, 1966). A two-layer structure renders less atomic shuffling than the four-layer structure, although at the expense of a larger shear per layer (Serra *et al.* 1991; Wang *et al.* 2010). Wang *et al.* (2010) aimed to determine the elementary structure of a $\{10\bar{1}1\}$ twinning dislocation using density functional theory and molecular dynamics (MD) simulation. A topological analysis revealed that a four-layer twinning dislocation could be constructed by two two-layer twinning dislocations. MD simulations confirmed that the dissociation of a basal dislocation

[1]However, we would like to note that when basal dislocations dissociations occur in succession, energetic considerations would suggest that these two systems of basal dislocations alternately interact with the twin boundary in order to eliminate the screw dislocation strain field.

Table 1. The specific combinations of mixed basal dislocations b_m and primary–secondary twin systems involved in the proposed double twinning mechanism. The basal glide plane is $(000\bar{1})$.

zone axis	**B**	$\mathbf{B_e}$	primary twin	secondary twin (type 1)	secondary twin (type 2)
$\pm[1\bar{2}10]$	$\pm\frac{1}{3}[\bar{2}110]$	$\frac{1}{3}[10\bar{1}0]$	$(10\bar{1}1)[\bar{1}012]$	$(\bar{1}01\bar{2})[10\bar{1}\bar{1}]$	$(\bar{1}012)[10\bar{1}1]$
	$\pm\frac{1}{3}[\bar{1}\bar{1}20]$				
$\pm[1\bar{2}10]$	$\pm\frac{1}{3}[\bar{2}110]$	$\frac{1}{3}[\bar{1}010]$	$(\bar{1}011)[10\bar{1}2]$	$(10\bar{1}\bar{2})[\bar{1}01\bar{1}]$	$(10\bar{1}2)[\bar{1}011]$
	$\pm\frac{1}{3}[\bar{1}\bar{1}20]$				
$\pm[\bar{2}110]$	$\pm\frac{1}{3}[1\bar{2}10]$	$\frac{1}{3}[01\bar{1}0]$	$(01\bar{1}1)[0\bar{1}12]$	$(0\bar{1}1\bar{2})[01\bar{1}\bar{1}]$	$(0\bar{1}12)[01\bar{1}1]$
	$\pm\frac{1}{3}[\bar{1}\bar{1}20]$				
$\pm[\bar{2}110]$	$\pm\frac{1}{3}[1\bar{2}10]$	$\frac{1}{3}[0\bar{1}10]$	$(0\bar{1}11)[01\bar{1}2]$	$(01\bar{1}\bar{2})[0\bar{1}1\bar{1}]$	$(01\bar{1}2)[0\bar{1}11]$
	$\pm\frac{1}{3}[\bar{1}\bar{1}20]$				
$\pm[\bar{1}\bar{1}20]$	$\pm\frac{1}{3}[\bar{2}110]$	$\frac{1}{3}[\bar{1}100]$	$(\bar{1}101)[1\bar{1}02]$	$(1\bar{1}0\bar{2})[\bar{1}10\bar{1}]$	$(1\bar{1}02)[\bar{1}101]$
	$\pm\frac{1}{3}[\bar{1}2\bar{1}0]$				
$\pm[\bar{1}\bar{1}20]$	$\pm\frac{1}{3}[\bar{2}110]$	$\frac{1}{3}[1\bar{1}00]$	$(1\bar{1}01)[\bar{1}102]$	$(\bar{1}10\bar{2})[1\bar{1}0\bar{1}]$	$(\bar{1}102)[1\bar{1}01]$
	$\pm\frac{1}{3}[\bar{1}2\bar{1}0]$				

at a $\{10\bar{1}1\}$ twin boundary produced a two-layer twinning dislocation (Wang *et al.* in press). Regarding kinetics, the energy barrier to move the two-layer twinning dislocation was substantially (more than four times) smaller than that to move the four-layer one (Serra *et al.* 1991; Wang *et al.* 2011*a*).[2] Based on these results, in the calculations to follow, we will consider that elementary twinning dislocations for $\{10\bar{1}1\}$ and $\{10\bar{1}2\}$ twins are two layers thick ($n=2$). With this established, magnitudes of s_1 and s_2 can be calculated with the following formulae for an HCP crystal with a given $\kappa = c/a$ (Yoo 1969, 1981; Wang *et al.* 2011*a*)

$$|s_1| = \frac{4\kappa^2 - 9}{3 + 4\kappa^2} \quad \text{and} \quad |s_2| = \frac{3 - \kappa^2}{3 + \kappa^2}. \tag{2.1}$$

For Mg, $\kappa = 1.623$ and $s_1 = -0.1135$ and $s_2 = 0.0649$. We choose to assign a sign to s_1 and s_2 to account for the fact that $\{10\bar{1}1\}$ and $\{10\bar{1}2\}$ twins have opposing stress sense in Mg.

3. Proposed mechanism for type 1 and type 2 double twin variants

Consider a pre-existing $\{10\bar{1}1\}$ primary twin. The mechanism for the nucleation of a type 1 or type 2 secondary $\{10\bar{1}2\}$ twin within the primary twin domain can be rationalized by a sequence of three dissociation reactions of slip dislocations occurring at the primary $\{10\bar{1}1\}$ twin boundary. The slip dislocations will likely be basal dislocations that originate within the primary twin, because basal slip is

[2]To completely understand the preference for the two-layer twinning dislocation seen in these MD simulations, however, requires studying the differences in their core energies.

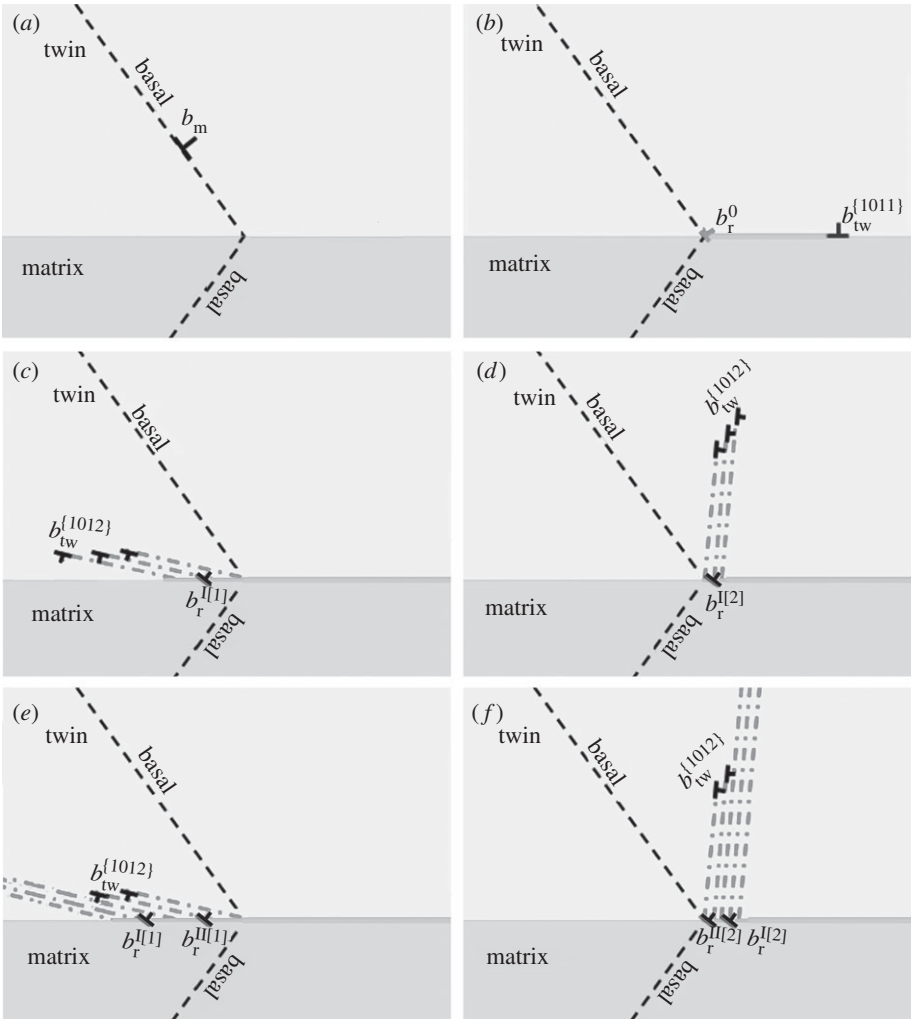

Figure 3. (a, b) Stage 1: (a) a mixed basal dislocation (b_m) originating within the primary twin (b) dissociates at the primary $(10\bar{1}1)$ twin boundary to produce a residual dislocation b_r^0 and a $(10\bar{1}1)$ twinning partial $b_{tw}^{(1011)}$ that can glide along the primary twin boundary. (c, d) Stage 2: reaction of a mixed basal dislocation with a residual dislocation b_r^0 has produced a residual b_r^I and three $\{10\bar{1}2\}$ twinning partials for (c) type 1 $(10\bar{1}2)$ and (d) type 2 $(10\bar{1}2)$ double twinning. (e, f) Stage 3: dissociation of a mixed basal dislocation into a residual b_r^{II} and two $\{10\bar{1}2\}$ twinning partials for (e) type 1 $(10\bar{1}2)$ and (f) type 2 $(10\bar{1}2)$ double twinning.

the easiest slip mode in Mg. It is implicitly assumed that the primary $\{10\bar{1}1\}$ twin domain has grown sufficiently thick to support the nucleation and glide of basal dislocations. This assumption still permits a secondary twin to form even within a primary twin that is too thin (tens of nanometre) to significantly contribute to strain accommodation. These three reactions make up three stages, which are illustrated in figure 3. Below, we present these reactions and carry out the corresponding energetic calculations.

(*a*) *Stage one: storage of defects on the primary twin boundary*

Consider a relatively large portion of the twin boundary containing little to no defects. When a basal dislocation originating from within the primary twin glides to and encounters this part of the twin boundary (figure 3*a*), it will dissociate into a glissile $\{10\bar{1}1\}$ twinning partial $b_{\mathrm{tw}}^{(10\bar{1}1)}$ of the same variant as the primary twin boundary and an immobile residual dislocation b_{r}^{0} (Wang *et al.* in press; figure 3*b*). The mixed basal dislocation **B**, residual defect b_{r}^{0} and twinning dislocation $b_{\mathrm{tw}}^{(10\bar{1}1)}$ share the same zonal axis as that of the primary twin boundary. This reaction can be expressed generally for all six variants of the primary twin boundary as

$$\mathbf{B} \Rightarrow b_{\mathrm{r}}^{0} + b_{\mathrm{tw}}^{(10\bar{1}1)}, \tag{3.1}$$

where $b_{\mathrm{r}}^{0} = \mathbf{B} - s_1[3\mathbf{B_e} - 2\mathbf{C}]$ and $b_{\mathrm{tw}}^{(10\bar{1}1)} = s_1[3\mathbf{B_e} - 2\mathbf{C}]$.

Satisfying constraints (i) and (iii) described in §2 leaves only one orientation of $\mathbf{B_e}$ for each variant of the $\{10\bar{1}1\}$ twin boundary. $\mathbf{B_e}$ can take one of two possible signs, i.e. $\pm\mathbf{B_e}$. If $+\mathbf{B_e}$ produces a twinning dislocation that would advance the boundary in one direction (say, thickening the twin), then $-\mathbf{B_e}$ would produce a partial that would advance the boundary in the other direction (shrinking the twin). Table 1 lists the two basal dislocations and corresponding $\mathbf{B_e}$ for each of the six primary twin variants.

The elastic interaction between the residual and twinning dislocations is repulsive, an outcome that helps to drive the dissociation and the twinning dislocation away from the residual dislocation. Without nearby obstacles, the glissile $b_{\mathrm{tw}}^{(10\bar{1}1)}$ twinning dislocation can propagate along the twin boundary (figure 3*a*,*b*), provided that a sufficiently high resolved shear stress is present to overcome the Peierls barrier (Wang *et al.* 2011*a*). The propagation of the twinning dislocation migrates the boundary (by two layers) and leaves the twin boundary energy unchanged. The residual dislocation stored at the boundary is much smaller than the original basal dislocation. The energetic favourability and feasibility of this reaction has been validated by MD (Wang *et al.* in press).

The primary twin thickens as this reaction occurs repeatedly in succession. Each reaction produces a glissile $b_{\mathrm{tw}}^{(10\bar{1}1)}$ dislocation that, under a suitable resolved shear stress, glides on the current twin boundary, advancing it a few additional layers. Several successive dissociations will at the same time leave the twin boundary defective with a distribution of residual dislocations b_{r}^{0}.

(*b*) *Stage two: formation of a stable secondary twin nucleus*

At some stage in primary twin growth, glide of newly created $b_{\mathrm{tw}}^{(10\bar{1}1)}$ dislocations will be resisted by the residual dislocations b_{r}^{0} left behind from previous reactions or other obstacles lying in the twin boundary. Hardening of the twin boundary in this way limits the mobility of $b_{\mathrm{tw}}^{(10\bar{1}1)}$ twinning dislocations and hinders primary twin boundary migration. Consequently, subsequent dissociation reactions producing $b_{\mathrm{tw}}^{(10\bar{1}1)}$ will no longer be favoured (as in stage one). In this event, basal slip dislocations could potentially pile up at the twin boundary. We propose that both the stress field that is generated by a pile up and the distribution of stored residual b_{r}^{0} dislocations may be relieved by secondary $\{10\bar{1}2\}$

twinning. Activating $\{10\bar{1}2\}$ twinning allows the material to accommodate the applied strain while overcoming residual defects that have accumulated in the primary twin boundary.

The mechanism for secondary $\{10\bar{1}2\}$ twinning builds on previous atomic-scale studies on the nucleation and glide of $\{10\bar{1}2\}$ twinning dislocations in Mg (Wang *et al.* 2009*a*,*b*). Atomistic calculations show that at least three $\{10\bar{1}2\}$ twinning partials must glide simultaneously on adjacent planes in order to form a $\{10\bar{1}2\}$ twin nucleus that is stable in a perfect HCP crystal. Individual $\{10\bar{1}2\}$ twinning dislocations, in contrast, can glide only adjacent to a pre-existing $\{10\bar{1}2\}$ twin boundary (Serra & Bacon 1996; Wang *et al.* 2009*a*,*b*). For secondary $\{10\bar{1}2\}$ twinning, we must, therefore, assume the following: (i) three twinning partials are sufficient to create a stable twin nucleus that can propagate into the primary twin away from the primary twin boundary and (ii) once the secondary twin nucleus has created two new twin boundaries within the primary twin, secondary twin thickening occurs by glide of a single or a pair of secondary twinning partials on planes adjacent to these new twin boundaries.

It can be shown that the requisite three $b_{\mathrm{tw}}^{(1012)}$ for a stable $\{10\bar{1}2\}$ twin nucleus cannot be obtained from the dissociation of a single basal dislocation. A three-layer $\{10\bar{1}2\}$ twin nucleus can, however, form when basal dislocations react with a pre-existing b_{r}^{0} as shown in figure 3*c*,*d*. (Alternatively, two closely spaced neighbouring residuals b_{r}^{0} can combine under mechanical loading and/or thermal activation and dissociate into a three-layer $\{10\bar{1}2\}$ twin nucleus.) The reacting basal dislocations and the product twinning dislocations must share the same zone axis. Only the two secondary twin systems that create type 1 and type 2 double twin variants (figures 1*a* and 2) satisfy this constraint. Figure 3 illustrates the formation of the three-layer $\{10\bar{1}2\}$ twin nucleus of type 1 (figure 3*c*) and type 2 (figure 3*d*). These two dissociation reactions are provided by

$$\textbf{type 1}: \quad \mathbf{B} + b_{\mathrm{r}}^{0} \Rightarrow b_{\mathrm{r}}^{\mathrm{I}[1]} + 3b_{\mathrm{tw}}^{(1012)[1]} \tag{3.2}$$

and

$$\textbf{type 2}: \quad \mathbf{B} + b_{\mathrm{r}}^{0} \Rightarrow b_{\mathrm{r}}^{\mathrm{I}[2]} + 3b_{\mathrm{tw}}^{(1012)[2]}. \tag{3.3}$$

The first leads to a type 1 double twin (figure 3*c*) and the second, a type 2 double twin (figure 3*d*). The Burgers vector for the type 1 secondary twin dislocation is $b_{\mathrm{tw}}^{(1012)[1]} = s_2[3\mathbf{B_e} - \mathbf{C}]$ and for type 2 $b_{\mathrm{tw}}^{(1012)[2]} = s_2[3\mathbf{B_e} + \mathbf{C}]$. The residual dislocation b_{r}^{I} (figure 3*c*,*d*) remaining at the boundary depends on whether type 1 or type 2 nucleated. These are

$$b_{\mathrm{r}}^{\mathrm{I}[1]} = 2\mathbf{B} - s_1[3\mathbf{B_e} - 2\mathbf{C}] - 3s^2[3\mathbf{B_e} - \mathbf{C}]$$

and

$$b_{\mathrm{r}}^{\mathrm{I}[2]} = 2\mathbf{B} - s_1[3\mathbf{B_e} - 2\mathbf{C}] - 3s^2[3\mathbf{B_e} + \mathbf{C}].$$

The interaction between b_{r}^{I} and the $3b_{\mathrm{tw}}^{(1012)}$ is repulsive for both types, an attribute that aids the initial expansion of the secondary $\{10\bar{1}2\}$ twin.

If provided adequate stress, the three-layer $\{10\bar{1}2\}$ twin nucleus can expand into the primary twin domain, circumventing the other residual dislocations (or obstacles) lying on the primary twin boundary. The result is less defect storage in the twin boundary, because the residual b_{r}^{I} left behind is much smaller than the original $b_{\mathrm{r}}^{0}+\mathbf{B}$. When the $\{10\bar{1}2\}$ twin nucleus expands into the primary $\{10\bar{1}1\}$ twin domain, it creates a pair of new $\{10\bar{1}2\}$ twin boundaries in an otherwise perfect crystal (figure 3). Because of this, large local stresses will be required for initial expansion of the secondary $\{10\bar{1}2\}$ twin.

(*c*) *Stage three: secondary twin growth by successive dissociations*

Once a secondary twin nucleus has propagated into the primary twin and formed new $\{10\bar{1}2\}$ twin boundaries, it can laterally expand by the glide of single and pairs of $\{10\bar{1}2\}$ twinning dislocations of the same variant on twin planes adjacent to its boundary. Glide of one $\{10\bar{1}2\}$ twinning dislocation advances the $\{10\bar{1}2\}$ twin domain by two layers (Serra & Bacon 1996; Wang *et al.* 2009*a*,*b*). This action is energetically favourable as no new boundary is created. Additional $\{10\bar{1}2\}$ twinning partials can be provided by the dissociation of basal slip dislocations that intersect the $\{10\bar{1}2\}$ twin boundary and split into $\{10\bar{1}2\}$ twinning partials. Each basal dislocation can dissociate into a pair of $\{10\bar{1}2\}$ twinning partials and a small residual dislocation $b_{\mathrm{r}}^{\mathrm{II}}$ (figure 3*e*,*f*) following

$$\textbf{type 1}: \quad \mathbf{B} \Rightarrow b_{\mathrm{r}}^{\mathrm{II}[1]} + 2b_{\mathrm{tw}}^{(10\bar{1}2)[1]} \quad (\text{figure } 3e) \tag{3.4}$$

and

$$\textbf{type 2}: \quad \mathbf{B} \Rightarrow b_{\mathrm{r}}^{\mathrm{II}[2]} + 2b_{\mathrm{tw}}^{(10\bar{1}2)[2]} \quad (\text{figure } 3f), \tag{3.5}$$

where $b_{\mathrm{r}}^{\mathrm{II}[1]} = \mathbf{B} - 2s_2[3\mathbf{B_e} - \mathbf{C}]$ and $b_{\mathrm{r}}^{\mathrm{II}[2]} = \mathbf{B} - 2s_2[3\mathbf{B_e} + \mathbf{C}]$.

This third reaction is likely, as indicated by MD simulation (Serra & Bacon 1996). The interaction between the product partials $b_{\mathrm{r}}^{\mathrm{II}}$ and the pair $2b_{\mathrm{tw}}^{(10\bar{1}2)}$ is repulsive for type 1 and type 2. This would not be the case if more than two $b_{\mathrm{tw}}^{(10\bar{1}2)}$, say three $b_{\mathrm{tw}}^{(10\bar{1}2)}$, were assumed to be produced from the dissociation.

Table 1 provides the primary–secondary double twin systems that would result from this double twinning mechanism.

(*d*) *A few remarks*

The second stage in the proposed double twinning mechanism is clearly the most critical, as it dictates if and when *formation and expansion* of a secondary $\{10\bar{1}2\}$ twin nucleus is favoured over continued growth of the primary $\{10\bar{1}1\}$ twin. This stage also determines which of the two possible secondary twin variants is activated, type 1 or type 2. In comparison, the other two stages are energetically favourable. In §6, the favourability of reaction stage three (which thickens the secondary twin) over reaction stage one (which thickens the primary one) when both the primary and secondary twin boundaries are present will be discussed.

Depending on the alloying content, the stacking fault energy on the basal plane may change (Yasi *et al.* 2010), affecting whether or not basal dislocations are extended as two Shockley partials with a stacking fault width in-between. The double twinning mechanism proposed here does not change conceptually whether

the dissociations involve perfect **B** or Shockley partial $\mathbf{B_e}$ dislocations. When $\mathbf{B_e}$ replaces **B** in the reactions mentioned earlier, the residual dislocation becomes pure edge.

4. Energetic considerations for type 1 and type 2 double twin variants

The interaction between the product partials is not the only factor determining dissociation reaction energies and many additional elements need to be taken into account. A general expression for the total energy change per unit length dislocation associated with a dissociation reaction is

$$\frac{\Delta E}{L} = \Delta G_{\text{core}} + \Delta G_{\text{line}} + \sum_{i \neq j} W_{ij} + \gamma |r_{ij}| - (\tau - \tau_{\text{p}}) b_i |r_{ij}|, \tag{4.1}$$

where $|r_{ij}|$ are relative distances between partials i and j and γ is the $\{10\bar{1}2\}$ twin boundary energy. The first two terms are the change in core and elastic line energies of the dislocation(s) participating in the reaction. The third term is the interaction energy between the residual dislocation and twinning dislocations. The fourth term is associated with any new twin faults that are created by glide of the twinning partials. The last term is the work performed by the imposed stress, where the scalar τ is the resolved shear stress and τ_{p} is the Peierls barrier for the selected twin plane and along the corresponding twin direction (Serra *et al.* 1991; Wang *et al.* 2011*a*). Energetic terms that are proportional to twin volume and hence would become relevant after some amount of twin growth, such as strain energy in the twin, strain energy in the matrix associated with accommodation, or formation of a double twin–matrix boundary, are not included in equation (4.1).

In this work, our interest lies in determining the stresses required to propagate twinning dislocations resulting from the proposed dissociations. For this purpose, we can disregard ΔG_{core} and ΔG_{line}. The term ΔG_{core} determines if the reaction would occur in the first place under the conditions provided. It should include both the activation energy to split the dislocation core and reductions in core energy due to relaxation of the core structure. The term ΔG_{line} is straightforward to calculate and is found to be negligible (Hirth & Lothe 1982; Wang *et al.* 2011*a*).

(*a*) *Stage one: storage of defects on the primary twin boundary*

The energy change per unit length dislocation associated with primary twin boundary expansion after the dissociation in stage one is

$$\frac{\Delta E}{L} = W_{b_{\text{r}}/b_{\text{tw}}} - (\tau - \tau_{\text{p}}) b_{\text{tw}}^{(1011)} |r|. \tag{4.2}$$

The fourth term in (4.1) is not included in equation (4.2) because glide of $b_{\text{tw}}^{(1011)}$ along the twin boundary does not create new boundary. The first term in (4.2) is the interaction energy, which is

$$W_{b_{\text{r}}/b_{\text{tw}}} = \frac{K}{2\pi} (b_{\text{r}}^0 \cdot b_{\text{tw}}^{(1011)}) \log\left(\frac{|r|}{r_0}\right) + K \frac{(b_{\text{r}}^0 \cdot r)(b_{\text{tw}}^{(1011)} \cdot r)}{r^2}, \tag{4.3}$$

where K is $24.6\,10^6\,\mathrm{J\,m^{-2}}$ (Capolungo & Beyerlein 2008) and r is the relative position of b_{r}^0 and $b_{\mathrm{tw}}^{(10\bar{1}1)}$. The second term in equation (4.2) is the work performed by the applied loading through a stress τ resolved on the twin plane and in the direction of the $\{10\bar{1}1\}$ twin. Solving for τ_{c}, the threshold τ obtained by setting $\Delta E = 0$ in equation (4.2), finds that $(\tau - \tau_{\mathrm{p}})$ is on the order of 1 MPa for r greater than a few $b_{\mathrm{tw}}^{(10\bar{1}1)}$. It decreases rapidly as the $\{10\bar{1}1\}$ twin partial glides away from the reaction site. Because such stresses are easily met, primary twin boundary migration after the dissociation event is likely.

(*b*) *Stage two: formation of a stable secondary twin nucleus*

The second dissociation reaction leads to a stable three-layer secondary $\{10\bar{1}2\}$ twin nucleus of one of two possible variants that share the same zonal axis as the primary twin. For either variant, the energy change associated with first expansion of the secondary $\{10\bar{1}2\}$ twin nucleus can be expressed generally as

$$\frac{\Delta E}{L} = W_{b_{\mathrm{r}}/b_{\mathrm{tw}}} + 2\gamma|r| - 3(\tau - \tau_{\mathrm{p}})\, b_{\mathrm{tw}}^{(10\bar{1}2)}|r|, \tag{4.4}$$

where r is defined as the distance between $b_{\mathrm{r}}^{\mathrm{I}}$ and $b_{\mathrm{tw}}^{(10\bar{1}1)}$. The first term is the interaction energy, which follows the same form as equation (4.3) but with b_{r}^0 and $b_{\mathrm{tw}}^{(10\bar{1}2)}$ in place of b_{r}^1 and $b_{\mathrm{tw}}^{(10\bar{1}1)}$, respectively. The second term is associated with the formation energy of a new set of $\{10\bar{1}2\}$ boundaries of length r. Given $\gamma = 122.3\,\mathrm{mJ\,m^{-2}}$ (Wang *et al.* 2009*a*) and $r/r_0 = 2$, one finds that this term dominates the first term by a few orders of magnitude. The last term is the work performed by mechanical forces. Solving equation (4.2) for τ_{c}, the value of τ yielding $\Delta E = 0$, indicates that the local shear resolved on the twinning dislocations needed to spread the initial $\{10\bar{1}2\}$ twin fault into the primary twin domain is significant, approximately 600 MPa above the Peierls stress.[3] According to equation (4.4), nuclei containing more than three $b_{\mathrm{tw}}^{(10\bar{1}2)}$, will require less stress, e.g. approximately 300 MPa for a six-layer nuclei.[4] In general, such large local stress states are required only for first expansion of the twin nucleus and can be supplied by local defects or pile ups. As will be shown next, subsequent growth requires substantially lower stresses.

Under a given stress state, the resolved shear stresses of type 1 and type 2 secondary twin variants are generally not the same. Both formation of a secondary $\{10\bar{1}2\}$ twin and whether it is type 1 or type 2, therefore, depend on the local stress field, that is, if, when, and on which variant, a sufficiently high τ is first generated (i.e. $\tau > \tau_{\mathrm{c}} + \tau_{\mathrm{p}}$).

[3]This approximation does not consider reductions in energy associated with relaxation of the core structure when a single large dislocation splits into several smaller dislocations.

[4]This calculation suggests that twinning dislocations may want to coalesce along the boundary to form a comparatively large twin nucleus before expanding into the primary twin for the first time. This pathway has been observed in MD simulations of $\{10\bar{1}2\}$ twin nucleation from symmetric tilt boundaries (Wang *et al.* 2010).

(c) Stage three: secondary twin growth by successive dissociations

Once a type 1 or type 2 secondary $\{10\bar{1}2\}$ twin boundary has been created, subsequent basal dislocations will dissociate spontaneously into $\{10\bar{1}2\}$ twinning dislocations of the same variant as that which created the initial fault. The energetic equation for $\{10\bar{1}2\}$ twin expansion is

$$\frac{\Delta E}{L} = W_{b_r/b_{tw}} - 2(\tau - \tau_p) b_{tw}^{(1012)} |r|. \tag{4.5}$$

For r greater than a few $b_{tw}^{(1012)}$, the threshold $(\tau_c - \tau_p)$ is 1 MPa or less, decreasing to zero as the $\{10\bar{1}2\}$ twinning partials glide along the secondary $\{10\bar{1}2\}$ twin boundary. Expansion of the secondary twin (figure 4) is thus substantially much easier than its nucleation. Clearly, if basal dislocations dissociate into $\{10\bar{1}2\}$ twinning dislocations at the secondary twin boundary rather than $\{10\bar{1}1\}$ twinning dislocations at the primary twin boundary (figure 3), then secondary twin growth would occur at the expense of primary twin growth.

Successive dissociation reactions by equation (4.5) lead to secondary twin growth. As the internal $\{10\bar{1}2\}$ twin spreads, the original $\{10\bar{1}1\}$ twin boundary becomes populated with residual dislocations. The uniform distribution of residuals will eventually rearrange and combine into fewer but larger defects, likely forming a faceted interface, in order to achieve coherency over greater portions of the boundary (Li *et al.* 2010). The resulting defect array is expected to cause the original $\{10\bar{1}1\}$ twin plane to tilt. In this event, the interface will experience some strain. Double twin planes have been observed to lie between $\{10\bar{1}1\}$ and $\{30\bar{3}4\}$ (Reed-Hill 1960; Yoshinaga *et al.* 1973; Cizek & Barnett 2008). The tilt may explain why the latter twin could not be predicted by Crocker's theory, which assumed *a priori* an invariant plane strain deformation, wherein the interface remains strain-free.

5. Dissociation reactions for type 3 and type 4 double twin variants

A description of secondary twin nucleation for types 3 and 4 requires a three-dimensional perspective. Following the same argument as for type 1 and type 2, secondary twins associated with type 3 and type 4 double twin variants nucleate when dislocations oriented along intersection lines Bf, Ac, cg and fh (defined in figure 1) dissociate into $\{10\bar{1}2\}$ twinning dislocations. As shown in figure 1*b–e*, these lines are non-parallel to the zone axis of the primary twin and have both ⟨c⟩ and ⟨a⟩ components. These traces also do not correspond to any of the traces formed between the twin boundary and all known HCP slip planes. Consequently, formation of the type 3 and type 4 variants must involve dissociations of mixed ⟨c + a⟩ dislocations that upon meeting the primary twin boundary locally reorient to align along one of these intersection lines. This manoeuvre requires dislocation climb because the intersection lines are non-parallel to the $\langle 11\bar{2}3\rangle$ Burgers vector.

The possible candidates for the dissociating ⟨c + a⟩ dislocations are first-order pyramidal ⟨c + a⟩ slip $\{10\bar{1}1\}\langle 11\bar{2}3\rangle$ and second-order pyramidal ⟨c + a⟩ slip $\{11\bar{2}2\}\langle 11\bar{2}3\rangle$, the two slip modes for accommodating *c*-axis deformation in an Mg crystal (Partridge 1967; Yoo & Wei 1967; Stohr & Poirier 1972; Obara *et al.* 1973;

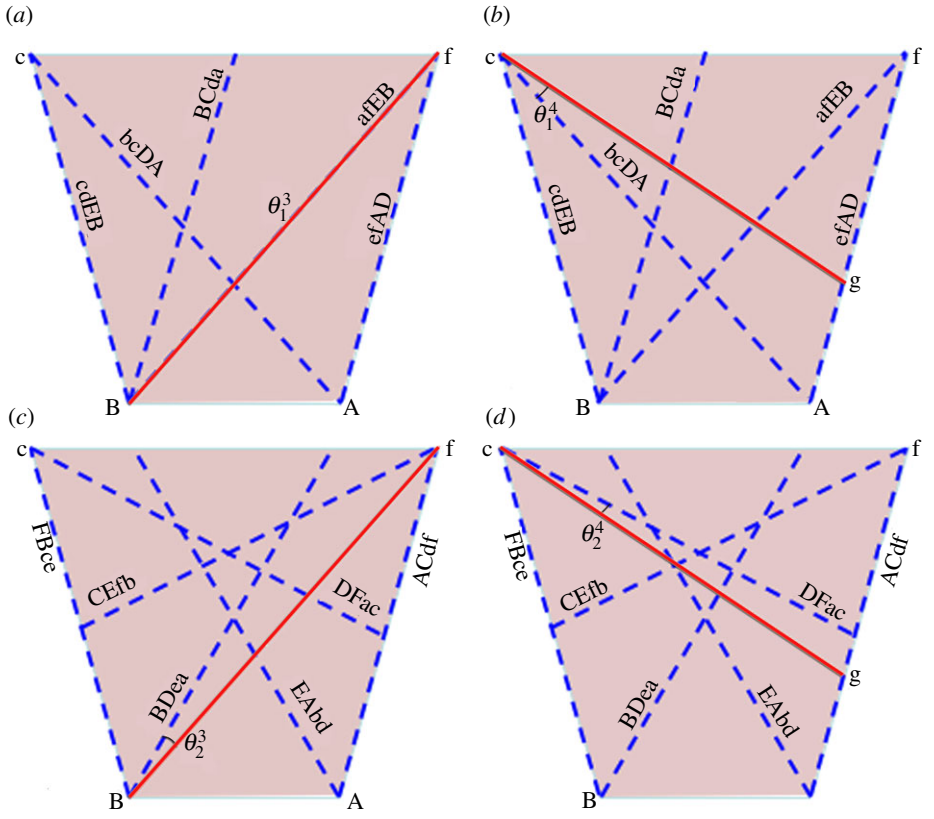

Figure 4. Blue dashed intersection lines of pyramidal ⟨c + a⟩ slip planes with the primary twin boundary (BAfc). (*a*) Intersection lines of the five first-order pyramidal planes $\{10\bar{1}1\}$ with primary twin plane and (*b*) intersection lines of the six second-order pyramidal planes $\{11\bar{2}2\}$ with primary twin plane relative to the desired intersection line *Bf* in red (figure 1*b*) for type 3 secondary twinning. (*c*) Intersection lines of the five $\{10\bar{1}1\}$ slip planes with the primary twin plane and (*d*) intersection lines of the six $\{11\bar{2}2\}$ slip planes with the primary twin plane relative to the desired intersection line *cg* in red (figure 1*d*) for type 4 secondary twinning. θ_i^j is the minimum angle between the slip plane intersection line (blue dashed) and the desired secondary twin plane intersection line (red solid). The subscript i is 1 or 2 corresponding to a first- or second-order pyramidal plane and the superscript j is 3 or 4 referring to type 3 or 4. For Mg, $\theta_1^3 = 0°$, $\theta_2^3 = 10.67°$, $\theta_1^4 = 14.46°$ and $\theta_2^4 = 8.62°$.

Ando & Tonda 2000). The model does not include the first-order pyramidal ⟨c + a⟩ slip system that shares the same plane as the primary twin boundary. It is doubtful that the ⟨c + a⟩ dislocations will originate from the twin boundary plane, either as a first-order pyramidal slip dislocation or a second-order pyramidal screw dislocation that has cross slipped onto the $\{10\bar{1}1\}$ twin boundary, because the $\{10\bar{1}1\}$ twin boundary favours the glide of $\{10\bar{1}1\}$ twinning dislocations over the larger ⟨c + a⟩ dislocations.

The local reorientation required for secondary twinning depends on the orientation relationship between the interacting slip and secondary twin systems and c/a ratio κ. Figure 4 compares the intersection traces of the five $\{10\bar{1}1\}$ slip

planes and the six $\{11\bar{2}2\}$ slip planes with the primary boundary with the desired intersection trace Bf for type 3 and cg for type 4. As shown, these dislocation lines are not parallel to the desired intersection lines Bf (figure 4*a*,*b* for type 3) or cg (figure 4*c*,*d* for type 4). To quantify this deviation, we introduce θ_i^j, the minimum angle between the dislocation line and the desired intersection line. The subscript i is 1 or 2 for first- or second-order pyramidal planes, respectively, and the superscript j is 3 or 4 corresponding to the double twin type. For type 3, the deviation θ_i^j as a function of κ is

$$\theta_1^3 = 0 \tag{5.1}$$

for the first-order pyramidal system coinciding with the twin boundary and

$$\theta_2^3 = \cos^{-1}\left[\frac{9+4\kappa^2}{2\sqrt{(3+\kappa^2)(7+4\kappa^2)}}\right], \tag{5.2}$$

where $\theta_2^3 = 10.67^\circ$ for Mg. For type 4, this deviation is

$$\theta_1^4 = \cos^{-1}\left[\frac{9+2\kappa^2}{2\sqrt{(3+\kappa^2)(7+\kappa^2)}}\right], \tag{5.3}$$

for the first-order pyramidal systems non-coplanar to the twin boundary and

$$\theta_2^4 = \cos^{-1}\left[\frac{19+2\kappa^2}{2\sqrt{(7+\kappa^2)(13+\kappa^2)}}\right]. \tag{5.4}$$

For Mg, $\theta_1^4 = 14.46^\circ$ and $\theta_2^4 = 8.62^\circ$ (figure 4). Because for the cases of interest, i.e. equations (5.2)–(5.4), the $\langle c+a\rangle$ dislocation must climb in order to be properly aligned for the dissociation, smaller θ_i^j is expected to favour secondary twinning.

The Burgers vector b_{py} of these $\langle c+a\rangle$ dislocations $[\mathbf{B}\pm\mathbf{C}]$ is large compared with that of a basal dislocation **B** or twinning dislocation. Consequently, provided all conditions mentioned earlier are met, they can dissociate into multiple $\{10\bar{1}2\}$ twinning dislocations via the following reaction:

$$b_{py} \Rightarrow b_r + 10\, b_{tw}^{(1012)}, \tag{5.5}$$

where the residual dislocation is

$$b_r = [\mathbf{B}\pm\mathbf{C}] - 10s_2[3\mathbf{B_e}\pm\mathbf{C}]. \tag{5.6}$$

The reaction (5.5) produces a stable $\{10\bar{1}2\}$ twin nucleus of type 3 or type 4 depending on its orientation (whether Bf and Ac for type 3 or cg and fh for type 4 in figure 1). Ten partials are predicted because the interaction between the residual b_r and a group of $10b_{tw}^{(1012)}$ is repulsive. This is not the case for dissociations producing 11 or more $\{10\bar{1}2\}$ twinning dislocations.

The $\{10\bar{1}2\}$ nucleus produced in equation (5.5) must then propagate into the primary twin domain and create a new $\{10\bar{1}2\}$ twin boundary. As with type 1 and type 2 double twinning, this initial expansion of the nucleus requires that

the resolved shear stress τ on the twin variant be sufficiently high. The stress τ to support this can be estimated by considering the energetics of the process, i.e.

$$\frac{\Delta E}{L} = W_{b_r/b_{tw}} + 2\gamma|r| - 10(\tau - \tau_p)b_{tw}^{(10\bar{1}2)}|r|, \tag{5.7}$$

where the value of τ, the resolved shear stress on the twin system, depends on whether type 3 or 4 is being considered. At this length scale, contributions to τ from local stresses generated by surrounding discontinuities or defects are just as, if not more, important than those from the applied stress (i.e. Schmid factor). Accordingly, both internal and applied stresses will influence whether type 3 or type 4 prevails. Once the initial fault has been created, secondary twin growth can proceed by production of more twinning dislocations via successive dissociations of pyramidal slip dislocations at the twin boundary.

6. Discussion

Experimentally, the type 1 secondary twin variant is observed to occur most often, even in the event that the other types, 2–4, are more favourably oriented with respect to the applied stress (Barnett *et al.* 2008; Martin *et al.* 2010). In these works, explanations for type 1 predominance have been based on strain accommodation and geometry, factors that are relevant when the secondary twin has already grown to an appreciable size. We offer insight into how the critical stages of secondary twin nucleation and initial expansion affect variant selection.

We propose that during deformation, secondary twins belonging to type 1–4 double twin variants can be created as a result of reactions between slip dislocations, originating from within the primary twin and the primary twin boundary. The mechanism for all four possible crystallographic structures of $\{10\bar{1}1\}-\{10\bar{1}2\}$ double twin variants can be generally described as proceeding through three stages: (i) a dissociation reaction that forms a stable secondary twin nucleus at the primary twin boundary, (ii) initial propagation of the nucleus into the primary twin to form a secondary twin, and (iii) successive dissociation reactions to expand this twin within the primary twin domain.

The dissociation reactions involved in the formation of type 1 and type 2 variants are, however, distinct from those associated with type 3 and type 4. The zone axis common to the primary twin and both type 1 and type 2 secondary twins lies parallel to $\langle a \rangle$ and thus has no $\langle c \rangle$ component. Because the orientation of mixed basal dislocations **B** is also parallel to this shared axis, it is possible for **B** to split to form type 1 and type 2 secondary twin dislocations needed for stages (i) and (iii). Stable nuclei of type 1 and type 2 variants can be created by the reaction of a mixed basal dislocation **B** with immobile defects b_r^0 remaining at the twin boundary as a result of previous reactions.[5] Both defects are likely to be present; basal slip is the easiest slip mode in Mg and b_r^0 remains from a highly favourable dissociation reaction involved in primary twin growth. Secondary twin planes corresponding to type 3 and type 4 double twin variants, in contrast, do not share a common zone axis with the primary

[5]Although not described here, we mention that stable nuclei can also form by the splitting of a couple of residual b_r^0 dislocations.

twin. As shown in figure 1*b–e*, the intersection lines made by each of these planes with the primary twin boundary have both ⟨c⟩ and ⟨a⟩ components. Type 3 and type 4 secondary twinning dislocations needed for stages (i) and (iii) are likely supplied by the dissociation of properly oriented pyramidal ⟨c + a⟩ slip dislocations at the twin boundary. Pyramidal ⟨c + a⟩ slip dislocations are zonal in structure, and substantially more difficult to activate and move than basal slip dislocations (Kronberg 1961; Rosenbaum 1964; Hutchinson 1977; Yoo 1981; Hirth & Lothe 1982). Thus, nucleation of types 3 and 4 is more complicated than that of types 1 and 2, because the former relies on the chance that hard-to-move ⟨c + a⟩ dislocations properly orient themselves (via climb) along the line of intersection between the primary twin boundary and secondary twin plane.

With the mechanism for double twinning clarified, the role of stress state on double twin variant selection can be understood. Two relevant stresses arise: the resolved shear stress (τ_s) on the slip dislocations that fuel the reactions at the twin boundaries, and the resolved shear stress (τ_{tw}) on the secondary twinning dislocations that are produced from these reactions. Recent reports of non-Schmid behaviour in double twin variant selection strongly suggest that τ_s and τ_{tw} should be calculated using the *local* stress state in the vicinity of the twin due to both the internal (e.g. pile ups) and applied stresses. In Barnett *et al.* (2008) and Martin *et al.* (2010), it was shown that type 1 double twinning occurred most often, although it was not the one expected based on a Schmid factor analysis with respect to the externally applied load direction.

The glide dislocation stress τ_s is important for secondary twin nucleus formation (stage (i)) and sustained growth (stage (iii)). For types 1 and 2, a suitable amount of shear on the basal slip systems is needed to activate and drive basal dislocations to the primary twin boundary. Types 3 and 4, on the other hand, require activation of ⟨c + a⟩ pyramidal slip, which, as already mentioned, is much more difficult than basal slip (Reed-Hill & Robertson 1957*b*; Beyerlein & Tomé 2008; Capolungo *et al.* 2009*a*,*b*). Because of their relatively high critical resolved shear stress (CRSS), a sufficiently high τ_s on the pyramidal slip systems must be present and/or basal slip must be unfavourable, in order for types 3 and 4 to form over types 1 and 2. The difference in CRSS between basal and pyramidal could give rise to a larger population of type 1 and 2 nuclei, rather than type 3 and 4 nuclei, at the primary twin boundary. The impact on growth stage (3) is that types 1 and 2 would thicken more easily than types 3 and 4. With all else being equal, a lower τ_s is required to *nucleate and thicken* types 1 and 2 twin variants than types 3 and 4 twin variants.

The second stress τ_{tw} is important for initial and continued expansion of the secondary twin (i.e. stages (ii) and (iii)). Among the four possible double twin types, the twin plane and twinning direction of type 1 is the most closely aligned with the twin plane and twinning direction of the primary twin (figures 1*a* and 2*a*), and type 4, the second most (Martin *et al.* 2010). The same local stress state that supports growth of the primary twin[6] will generate a τ_{tw} that favours creation of a new $\{10\bar{1}2\}$ twin fault (stage (ii)) and subsequent glide of $\{10\bar{1}2\}$ twinning dislocations on the type 1 twin plane (stage (iii)). In contrast, types

[6]The local stresses that nucleated the primary twin in the first place are likely relieved by it. Thus, the stresses that favour growth of the primary twin, not its nucleation, are those that will favour type 1 over type 2.

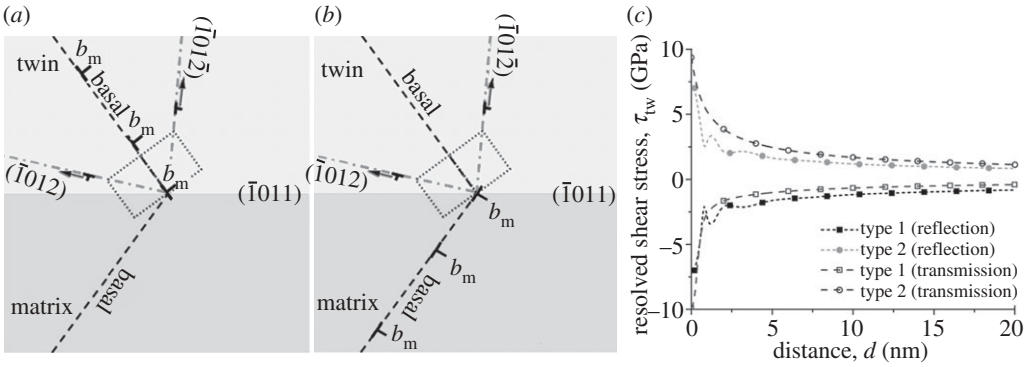

Figure 5. Schematic illustrating how a basal dislocation pile up, originating either from within the (*a*) primary twin, the 'reflection' case, or (*b*) matrix, the 'transmission' case, promotes secondary twins within the primary twin. (*c*) The resolved shear stress in the type 1 and type 2 twin planes for these two cases. The result indicates that a pile up in either case can promote nucleation of a type 2 over type 1 secondary twin variant.

2–4 must arise from a stress state that does not favour growth of the primary twin but could be encouraged if a pile up were to form at the primary twin boundary after some amount of straining. For example, consider a large pile up of basal dislocations at the primary twin boundary that originates either within the primary twin (figure 5*a*) or in the matrix (figure 5*b*). In the former case, the pile up produces a stress field that would promote twinning along the type 2 twin plane, thereby 'reflecting' a secondary twin back into the primary twin. Likewise, in the latter case, a basal pile up originating from the matrix generates a stress field that 'transmits' across the interface most effectively on the type 2 plane. The corresponding resolved shear stress on the type 1 and type 2 twin systems owing to the pile ups in these two cases are calculated using a stressed single dislocation pile-up model (Hirth & Lothe 1982) and shown in figure 5*c*. In this calculation, the pile up contains 20 basal dislocations, $\tau_{yx} = 100\,\mathrm{MPa}$, and $\sigma_{xx} - \sigma_{yy} = 188\,\mathrm{MPa}$, which leads to a resolved shear stress of 100 MPa on the primary twin boundary and 100 MPa on the basal plane. The results in figure 5*c* show that the pile up in both cases produces a τ_{tw} favourable to type 2. The pile up associated with the reflection case additionally favours type 2 over type 1 secondary twinning because it blocks the motion of type 1 $\{10\bar{1}2\}$ twinning dislocations, as illustrated in figure 5*a*. The additional requirement of a pile up (or similarly large defect) may explain why type 2 double twins are rarely observed at the micron scale (Barnett *et al.* 2008; Martin *et al.* 2010) or are considerably finer than the type 1 twin variant (Cizek & Barnett 2008).

For several reasons, it is likely that the onset of secondary twin growth marks the end of primary twin growth, which would also explain the thin lenticular morphology of double twins. Once secondary twinning initiates, dislocations interacting with the twin boundary are then presented with two types of twin boundaries: a secondary $\{10\bar{1}2\}$ twin boundary and the original primary $\{10\bar{1}1\}$ twin boundary. In this situation, a gliding basal dislocation can spontaneously dissociate either into a $\{10\bar{1}1\}$ twinning dislocation (which advances the primary twin boundary) or into a few $\{10\bar{1}2\}$ twinning dislocations (which advances the

secondary twin). Although both processes require little stress to drive them, the latter dissociation is expected to be more favourable. First, $\{10\bar{1}2\}$ twinning dislocations are more mobile than $\{10\bar{1}1\}$ twinning dislocations. First principle and MD simulations reveal that $\{10\bar{1}2\}$ twinning requires less distortional energy (smaller Burgers vector) and kinetic energy (less atomic shuffling) than $\{10\bar{1}1\}$ twinning (Wang *et al.* 2009*b*, 2011*a*). Second, $|b_{\mathrm{r}}^{\mathrm{II}}| < |b_{\mathrm{r}}^{0}|$, means that the dissociation into $\{10\bar{1}2\}$ twinning dislocations (figure 3*c*,*d*) leads to less defect storage in the primary twin boundary than the dissociation into $\{10\bar{1}1\}$ twinning dislocations (figure 2). Also, secondary twinning provides a mechanism for recovering the residual defects b_{r}^{0} accumulated after primary twin growth. Third, the effective twin shear supplied by the double twin is roughly 25 per cent greater than that of the primary twin (Crocker 1962; Mendelson 1970). When the component twins of the double twin share the same plane of shear, the double twin shear is provided by Crocker (1962)

$$g_{\mathrm{DT}} = \sqrt{g_1 g_2 (g_1 \sin\theta - 2\cos\theta)(g_2 \sin\theta - 2\cos\theta) - (g_1 - g_2)^2}, \tag{6.1}$$

where g_1 is the twin shear of the primary $\{10\bar{1}1\}$ twin and g_2 of the secondary $\{10\bar{1}2\}$ twin. For Mg, in which $\kappa = 1.623$ and $n = 2$, $g_1 = 0.4038$ and $g_2 = 0.129$ (Mendelson 1970; Yoo 1981; Wang *et al.* 2011*a*), giving $g_{\mathrm{DT}} = 0.4959$ for type 1 and $g_{\mathrm{DT}} = 0.2795$ for type 2. Hence, strain is more efficiently accommodated by thickening the secondary $\{10\bar{1}2\}$ twin than the primary twin. It follows directly from all considerations earlier that once secondary twinning begins, its growth is favoured over that of its host.

In summary, the occurrence and predominance of type 1 double twinning can be attributed to its relative ease for (i) nucleation, which involves the easiest slip mode, basal slip, (ii) propagation, which occurs by highly mobile $\{10\bar{1}2\}$ twinning dislocations, (iii) continuous growth, which is supported by basal slip and activated by the same local stress state that grew the primary twin, and (iv) supplying shear, which is higher than the twin shear of the primary twin and that of the type 2 double twin. Thus, the frequently observed type 1 variant has as much to do with nucleation as with growth. The other types are comparatively more difficult to nucleate and grow.

The focus of this study lies in the nucleation and initial stages of secondary twin growth. Growth of a secondary twin to a sizeable volume, sufficient to contribute to the applied strain, calls for additional considerations. For instance, an argument for the apparent favourability of type 1, compared with type 2, is that type 1 involves smaller rotations. Specifically, type 1 internal twinning leads to a small misorientation $\theta = 18.7^\circ$ between the basal planes of the parent and double twin, whereas type 2 leads to a significantly larger misorientation, $\theta = 75^\circ$ (Barnett *et al.* 2008; Martin *et al.* 2010). Also, type 1 involves a larger twin shear than type 2. According to equation (5.5), $g_{\mathrm{DT}} = 0.4959$ for type 1 and 0.2795 for type 2. Thus, a double twin band containing a type 2 internal twin will need to be nearly twice as large as one containing a type 1 internal twin to accommodate the same strain. We also mention that the structure and migration characteristics of the double twin boundary will depend on variant type and could play a role in which variant is visible in metallographic analyses.

Nucleation of the primary $\{10\bar{1}1\}$ twins is not dealt with in this work. Only very recently have atomic-scale studies, probability models and statistical analyses dedicated to nucleation and growth of $\{10\bar{1}2\}$ extension twins been carried out (Beyerlein & Tomé 2010; Beyerlein *et al.* 2010; Wang *et al.* 2010). These studies support the idea that twin nucleation originates at grain boundaries, a mechanism that is likely to apply to $\{10\bar{1}1\}$ twinning as well. Very recently, a theory has been proposed to explain the variant selection of primary compression twins (Jonas *et al.* 2011) based on grain boundary accommodation.

7. Conclusions

In this study, we propose that the nucleation and growth of a secondary $\{10\bar{1}2\}$ twin within a primary $\{10\bar{1}1\}$ twin can be understood based on a sequence of dissociations of slip dislocations into $\{10\bar{1}2\}$ twinning dislocations at the $\{10\bar{1}1\}$ twin boundary. According to the model, initiation of secondary twinning would hinder thickening of the host primary twin.

The mechanism for type 1 and type 2 secondary twinning involves the dissociation of basal slip dislocations. We suspect that whether type 1 or type 2 is activated is related to the presence and orientation of a pile up at the primary twin boundary. Without a pile up, type 1, whose secondary twin plane is more closely aligned with the $\{10\bar{1}1\}$ twin boundary, would be produced (figure 2). Otherwise, if a pile up of basal dislocations develops, then type 2 secondary twinning could be favoured (figure 5).

Formation of secondary twin nuclei of types 3 and 4 via a dislocation–dissociation mechanism is also possible, but is much more difficult, involving the dissociation of properly oriented pyramidal $\langle c + a \rangle$ dislocations. This distinction provides one reason why type 1 double twinning is overwhelmingly the most frequently observed double twin variant, because in Mg, $\langle c + a \rangle$ dislocations are much more difficult to activate and move than basal $\langle a \rangle$ slip dislocations.

Metallographic studies that establish correlations between double twin band thickness and secondary twin variant type are desirable. Three-dimensional MD simulations required to study the reactions proposed for types 3 and 4 double twin variants are also recommended.

I.J.B., J.W. and C.N.T. acknowledge full support for their work by the U.S. Department of Energy, Office of Basic Energy Sciences (project no: FWP-06SCPE401). M.R.B. thanks the ARC Centre of Excellence for Design in Light Metals for its support.

References

Akhtar, A. 1973 Compression of zirconium single crystals parallel to the *c*-axis. *J. Nucl. Mater.* **47**, 79–86. (doi:10.1016/0022-3115(73)90189-X)

Akhtar, A. & Teghtsoonian, A. 1971 Plastic deformation of zirconium single crystals. *Acta Metall.* **19**, 655–663. (doi:10.1016/0001-6160(71)90019-8)

Ando, S. & Tonda, H. 2000 Non-basal slip in magnesium-lithium alloy single crystals. *Mater. Trans. JIM* **41**, 1188–1191.

Ando, D., Koike, J. & Sutou, Y. 2010 Relationship between deformation twinning and surface step formation in AZ31 magnesium alloys. *Acta Mater.* **58**, 4316–4324. (doi:10.1016/j.actamat.2010.03.044)

Aydiner, C. C., Bernier, J. V., Clausen, B., Lienert, U., Tome, C. N. & Brown, D. W. 2009 Evolution of stress in individual grains and twins in a magnesium alloy aggregate. *Phys. Rev. B* **80**, 024113. (doi:10.1103/PhysRevB.80.024113)

Barnett, M. R., Keshavarz, Z., Beer, A. G. & Ma, X. 2008 Non-Schmid behaviour during secondary twinning in a polycrystalline magnesium alloy. *Acta Mater.* **56**, 5–15. (doi:10.1016/j.actamat.2007.08.034)

Beyerlein, I. J. & Tomé, C. N. 2008 A dislocation-based constitutive law for pure Zr including temperature effects. *Int. J. Plast.* **24**, 867–895. (doi:10.1016/j.ijplas.2007.07.017)

Beyerlein, I. J. & Tomé, C. N. 2010 A probabilistic twin nucleation model for HCP polycrystalline metals. *Proc. R. Soc. A* **466**, 2517–2544. (doi:10.1098/rspa.2009.0661)

Beyerlein, I. J., Capolungo, L., Marshall, P. E., McCabe, R. J. & Tomé, C. N. 2010 Statistical analyses of deformation twinning in magnesium. *Philos. Mag.* **90**, 2161–2190. (doi:10.1080/14786431003630835)

Beyerlein, I. J., McCabe, R. J. & Tomé, C. N. 2011 Effect of microstructure on the nucleation of deformation twins in polycrystalline in high-purity magnesium: a multi-scale modeling study. *J. Mech. Phys. Solids* **59**, 988–1003. (doi:10.1016/j.jmps.2011.02.007)

Bozzolo, N., Chan, L. & Rollett, A. D. 2010 Misorientations induced by deformation twinning in titanium. *Appl. Crystallogr.* **43**, 596–602. (doi:10.1107/S0021889810008228)

Capolungo, L. & Beyerlein, I. J. 2008 Nucleation and stability of twins in hcp metals. *Phys. Rev. B* **78**, 024117. (doi:10.1103/PhysRevB.78.024117)

Capolungo, L., Beyerlein, I. J. & Tomé, C. N. 2009*a* Slip-assisted twin growth in hexagonal close-packed metals. *Scr. Mater.* **60**, 32–25. (doi:10.1016/j.scriptamat.2008.08.044)

Capolungo, L., Marshall, P., McCabe, R. J., Beyerlein, I. J. & Tomé, C. N. 2009*b* Nucleation and growth of twins in Zr: a statistical study. *Acta Mater.* **57**, 6047–6056. (doi:10.1016/j.actamat.2009.08.030)

Christian, J.W. & Mahajan, S. 1995 Deformation twinning. *Prog. Mater. Sci.* **39**, 1. (doi:10.1016/0079-6425(94)00007-7)

Cizek, P. & Barnett, M. R. 2008 Characteristics of the contraction twins formed close to the fracture surface in Mg-3Al-1Zn alloy deformed in tension. *Scr. Mater.* **59**, 959–962. (doi:10.1016/j.scriptamat.2008.06.041)

Couling, S. L. & Roberts, C. S. 1956 New Twinning systems in magnesium. *Acta Crystallogr.* **9**, 972–973. (doi:10.1107/S0365110X56002758)

Couling, S. L., Pashak, J. F. & Sturkey, L. 1959 Unique deformation and aging characteristics of certain magnesium-base alloys. *Trans. Metall. Soc. AIME* **51**, 94–107.

Crocker, A. G. 1962 Double twinning. *Philos. Mag.* **83**, 1901–1924. (doi:10.1080/14786436208213854)

Hartt, W. H. & Reed-Hill, R. E. 1968 Internal deformation and fracture of second-order {1011}–{1012} twins in magnesium. *Trans. Metall. Soc. AIME* **242**, 1127–1133.

Hauser, F. E., Landon, P. R. & Dorn, J. E. 1956 Fracture of magnesium alloys at low temperature. *J. Metals Trans. AIME* **206**, 589–593.

Hirth, J. P. & Lothe, J. 1982 *Theory of dislocations*. Malabar, FL: Krieger Publishing Company.

Hutchinson, J. W. 1977 Creep and plasticity of hexagonal polycrystals as related to single crystal slip. *Metall. Mater. Trans. A Phys. Metall. Mater. Sci.* **8**, 1465–1469. (doi:10.1007/BF02642860)

Jonas, J. J., Mu, S., Al-Samman, T., Gottstein, G., Jiang, L. & Martin, E. 2011 The role of strain accommodation during the variant selection of primary twins in magnesium. *Acta Mater.* **59**, 2046–2056. (doi:10.1016/j.actamat.2010.12.005)

Koike, J., Fujiyama, N., Ando, D. & Sutou, Y. 2010 Roles of deformation twinning and dislocation slip in the fatigue failure mechanism of AZ31 Mg alloys. *Scr. Mater.* **63**, 747–750. (doi:10.1016/j.scriptamat.2010.03.021)

Kronberg, M. L. 1961 Atom movements and dislocation structures in some common crystals. *Acta Metall.* **9**, 970–972. (doi:10.1016/0001-6160(61)90124-9)

Li, B. & Ma, E. 2009 Atomic shuffling dominated mechanism for deformation twinning in magnesium. *Phys. Rev. Lett.* **103**, 035003. (doi:10.1103/PhysRevLett.103.035003)

Li, Y. J., Chen, Y. J., Walmsley, J. C., Mathinsen, R. H., Dumoulin, S. & Roven, H. J. 2010 Faceted interfacial structure of {10–11} twins in Ti formed during equal channel angular pressing. *Scr. Mater.* **62**, 443–446. (doi:10.1016/j.scriptamat.2009.11.039)

Martin, E., Capolungo, L., Jiang, L. & Jonas, J. J. 2010 Variant selection during secondary twinning in Mg–3%Al. *Acta Mater.* **58**, 3970–3983. (doi:10.1016/j.actamat.2010.03.027)

Mendelson, S. 1969 Zonal dislocations and twin lamellae in h.c.p. metals. *Mater. Sci. Eng.* **4**, 231–242. (doi:10.1016/0025-5416(69)90067-6)

Mendelson, S. 1970 Dislocation dissociation in hcp metals. *J. Appl. Phys.* **41**, 1893–1910. (doi:10.1063/1.1659139)

Obara, T., Yoshinaga, H. & Morozumi, S. 1973 {1122} ⟨1123⟩ slip system in magnesium. *Acta Metall.* **21**, 845–853. (doi:10.1016/0001-6160(73)90141-7)

Partridge, P. G. 1967 The crystallography and deformation modes of hexagonal close-packed metals. *Metall. Rev.* **12**, 168–194.

Pond, R. C. & Hirth, J. P. 1994 *Solid state physics academic*, vol. 47, p. 287. New York, NY: Plenum Press.

Pond, R. C., Bacon, D. J., & Serra, A. 1995 Interfacial structure of {1011} twins and twinning dislocations in titanium. *Philos. Mag. Lett.* **71**, 275. (doi:10.1080/09500839508240521)

Reed-Hill, R. E. 1960 Study of {1011} and {1013} twinning modes in magnesium. *Trans. Metall. Soc. AIME* **218**, 554–558.

Reed-Hill, R. E. & Robertson, W. D. 1957*a* Additional modes of deformation twinning in magnesium. *Acta Metall.* **5**, 717–727. (doi:10.1016/0001-6160(57)90074-3)

Reed-Hill, R. E. & Robertson, W. D. 1957*b* Crystallographic characteristics of fracture in magnesium single crystals. *Acta Metall.* **5**, 728–737. (doi:10.1016/0001-6160(57)90075-5)

Rosenbaum, H. S. 1964 *Nonbasal slip in hcp metals and its relation to mechanical twinning*. Newark, NJ: Gordon Breach.

Serra, A. & Bacon, D. J. 1996 A new model for {1012} twin growth in hcp metals. *Philos. Mag.* **73**, 333–343. (doi:10.1080/01418619608244386)

Serra, A., Bacon, D. J. & Pond, R. C. 1988 The crystallography and core structures of twinning dislocations in h.c.p. metals. *Acta Metall.* **12**, 3183–3203. (doi:10.1016/0001-6160(88)90054-5)

Serra, A., Pond, R. C. & Bacon, D. J. 1991 Computer simulation of the structure and mobility of twinning dislocations in hcp metals. *Acta Metall.* **39**, 1469–1480. (doi:10.1016/0956-7151(91)90232-P)

Serra, A., Bacon, D. J. & Pond, R. C. 2010 Comment on 'atomic shuffling dominated mechanism for deformation twinning in magnesium'. *Phys. Rev. Lett.* **104**, 029603. (doi:10.1103/PhysRevLett.104.029603)

Stohr, J. F. & Poirier, J. P. 1972 Etude en microscopie electronique du glissement pyramidal {1122} ⟨1123⟩ dans le magnesium. *Philos. Mag.* **25**, 1313–1329. (doi:10.1080/14786437208223856)

Thompson, N. & Millard, D. J. 1952 Twin formation in cadmium. *Phil. Mag.* **43**, 422–440.

Thornton, P. H. 1965 Pyramidal twinning, cleavage, and prismatic slip in the h.c.p. copper–germanium phase. *Acta Metall.* **13**, 611–622. (doi:10.1016/0001-6160(65)90123-9)

Thornton, P. H. 1966 Reply to discussion 'on {10.1} twinning in the hcp structure'. *Acta Metall.* **14**, 444. (doi:10.1016/0001-6160(66)90108-8)

Wang, J., Hoagland, R., Hirth, J. P., Capolungo, L., Beyerlein, I. J. & Tomé, C. N. 2009*a* Nucleation of (1012) twins in hexagonal close packed crystals. *Scr. Mater.* **61**, 903–906. (doi:10.1016/j.scriptamat.2009.07.028)

Wang, J., Hirth, J. P. & Tomé, C. N. 2009*b* (−1 0 1 2) twinning nucleation mechanisms in hexagonal-close-packed crystals. *Acta Mater.* **57**, 5521–5530. (doi:10.1016/j.actamat.2009.07.047)

Wang, J., Beyerlein, I. J. & Tomé, C. N. 2010 An atomic and probabilistic perspective on twin nucleation in Mg. *Scr. Mater.* **63**, 741–746. (doi:10.1016/j.scriptamat.2010.01.047)

Wang, J., Beyerlein, I. J., Hirth, J. P. & Tomé, C. N. 2011*a* Twinning dislocations on {−1011} and {−1013} planes in hexagonal close-packed crystals. *Acta Mater.* **59**, 3990–4001. (doi:10.1016/j.actamat.2011.03.024)

Wang, J., Beyerlein, I. J., Mara, N. A. & Bhattacharyya, D. 2011*b* Interface-facilitated deformation twinning in copper within submicron Ag–Cu multilayered composites. *Scr. Mater.* **64**, 1083–1086. (doi:10.1016/j.scriptamat.2011.02.025)

Wang, J., Beyerlein, I. J. & Hirth, J. P. In press. Nucleation of elementary {−1011} and {−1013} twinning dislocations at a twin boundary in hexagonal-close-packed crystals. *Model. Simul. Mater. Sci. Eng.* Online at stacks.iop.org/MSMSE/19

Westlake, D. G. 1961 Twinning in zirconium. *Acta Metall.* **9**, 327–331. (doi:10.1016/0001-6160(61)90226-7)

Westlake, D. G. 1966 On {10.1} twinning in the h.c.p. structure. *Acta Metall.* **14**, 442–444. (doi:10.1016/0001-6160(66)90107-6)

Wonsiewicz, B. C. & Backofen, W. A. 1967 Plasticity of magnesium crystals. *Trans. Metall. Soc. AIME* **239**, 1422.

Yasi, J. A., Hector, L. G. & Trinkle, D. R. 2010 First-principles data for solid-solution strengthening of magnesium: from geometry and chemistry to properties. *Acta Mater.* **58**, 5704–5713. (doi:10.1016/j.actamat.2010.06.045)

Yoo, M. H. 1969 Interaction of slip dislocations with twins in hcp metals. *Trans. Metall. Soc. AIME* **245**, 2051–2060.

Yoo, M. H. 1981 Slip, twinning, and fracture in hexagonal close-packed metals. *Metall. Mater. Trans. A Phys. Metall. Mater. Sci.* **12**, 409–418. (doi:10.1007/BF02648537)

Yoo, M. H. & Wei, C. T. 1967 Slip modes of hexagonal-close-packed metals. *J. Appl. Phys.* **38**, 4317–4322. (doi:10.1063/1.1709121)

Yoshinaga, H., Obara, T. & Morozumi, S. 1973 Twinning deformation in magnesium compressed along the c-axis. *Mater. Sci. Eng.* **12**, 255–264. (doi:10.1016/0025-5416(73)90036-0)